BIOCHEMISTRY
including biophysical chemistry & molecular biology
Article

Biochemistry **2009,** *48,* 10499–10508 10499
DOI: 10.1021/bi9011385

The Unstable Part of the Apical Stem of Duck Hepatitis B Virus Epsilon Shows Enhanced Base Pair Opening but Not Pico- to Nanosecond Dynamics and Is Essential for Reverse Transcriptase Binding[†]

Kirsten A. M. Ampt, Ramon M. van der Werf, Frank H. T. Nelissen, Marco Tessari, and Sybren S. Wijmenga*

Biophysical Chemistry, Institute of Molecules and Materials, Radboud University of Nijmegen, Heyendaalseweg 135, 6525 AJ Nijmegen, The Netherlands

Received July 6, 2009; Revised Manuscript Received September 21, 2009

ABSTRACT: Hepatitis B virus (HBV) replication starts with binding of reverse transcriptase (RT) to the apical stem−loop region of epsilon, a conserved element of the RNA pregenome. For duck HBV, an in vitro replication system has provided molecular details of this interaction. Further insights can be obtained from the structure and dynamics of the duck and human apical stem−loops. Previously, we reported these for the human apical stem−loop. Here, we present the same for the duck counterpart. Unlike its human counterpart, the duck apical stem is unstable in its middle/upper part and contains noncanonical base pairs. This dynamics study is the first of an unstable RNA−DNA stem. Similar to the human stem, the duck apical stem comprises two helical segments with a bend angle of ca. 10°, separated by a nonpaired mobile U residue. It is capped by a well-structured conserved UGUU loop with two residues mobile on the pico- to nanosecond time scale, one of which is involved in RT binding. Remarkably, the unstable middle/upper part of the stem does not show enhanced pico- to nanosecond time scale dynamics. Instead, adenine dispersion relaxation studies indicate enhanced millisecond time scale dynamics involving base pair opening. It can then be concluded that base pair opening is essential for epsilon−RT binding, because stabilization of the stem abolishes binding. We hypothesize that binding occurs by conformational capture of bases in the base pair open state. The unstable secondary structure of the apical stem−loop makes duck epsilon−RT binding unusual in light of recent classifications of RNA target interactions that assume stable secondary structures.

The hepatitis B virus (HBV)[1] is the most common cause of liver infection in the world, infecting mammalian as well as avian hosts. More than 300 million people worldwide are estimated to be chronically infected with HBV, and so far, no treatment for the efficient elimination of HBV in chronically infected patients exists (*1*−*3*). HBV is a member of the Hepadnaviridae family consisting of hepatotropic DNA viruses, which also includes related animal viruses such as duck HBV (DHBV) and heron HBV (HHBV). The hepadnaviral genome replication cycle consists of the following parts. (1) The genome, contained in infectious virions as small, 3.2 kb relaxed circular, partially double-stranded DNA (RC-DNA), enters the infected cell. (2) The RC-DNA is then converted inside the host cell nucleus into a plasmid-like covalently closed circular DNA (cccDNA). (3) Genomic and pregenomic RNAs (pg-RNA) are subsequently transcribed from the cccDNA by cellular RNA polymerase II. (4) Viral proteins, like the P-protein (see below), and viral coat proteins are translated from pgRNAs acting as mRNAs; the P-protein consists of a conserved reverse transcriptase domain (RT), a middle spacer, a C-terminal RNase H domain (RH), and at its N-terminus a terminal domain (TP). (5) The pgRNA contains near its 5′-end an important structurally conserved element, called epsilon (ε). ε is a ca. 60-nucleotide (nt) RNA fragment that folds into a lower stem and apical stem−loop region, separated by an ∼6 nt internal bulge. Binding of the RT domain of the P-protein to the apical stem−loop of ε triggers the packaging of the pgRNA into progeny capsids, after which a 4 nt DNA primer is synthesized using the 6 nt internal bulge of ε as a template; subsequently, the P-protein moves to the 3′-end of the pg-RNA, where reverse transcription by the P-protein starts and new RC-DNA is produced (*2*−*5*).

The conserved 60 nt ε RNAs of human and avian HBV and in particular their apical stem−loops (Figure 1) each form a crucial structural element in the replication of their respective HBVs, because binding of the RT domain of the P-protein to the conserved apical stem−loop of ε triggers the molecular events that lead to the reverse transcription of the pregenomic RNA. Many of the molecular details of the P−ε interaction leading up to the 4 nt primer synthesis have been established, thanks to a fully functional cell-free and chaperone-dependent reconstituted P−ε system based on duck HBV (*3*, *5*−*10*). An in vitro reconstituted system has also been developed for human HBV (*11*, *12*). It shows P−ε binding, but no primer synthesis, and provided ε sequence requirements for this binding and demonstrated the involvement of the RT domain in ε binding. Nevertheless, many molecular details of the P−ε interaction stem from the duck in vitro system, and a variety of biochemical experiments have been conducted (*3*, *5*−*10*), including SELEX experiments (*9*), in defining the sequence requirements crucial for

[†]This work was funded by the European sixth framework program, STREP Project FSG-V-RNA.

*To whom correspondence should be addressed. E-mail: s.wijmenga@science.ru.nl. Telephone: +31 24 3653384. Fax: +31 243652112.

[1]Abbreviations: HBV, hepatitis B virus; NMR, nuclear magnetic resonance; NOE, nuclear Overhauser effect.

Published on Web 10/09/2009

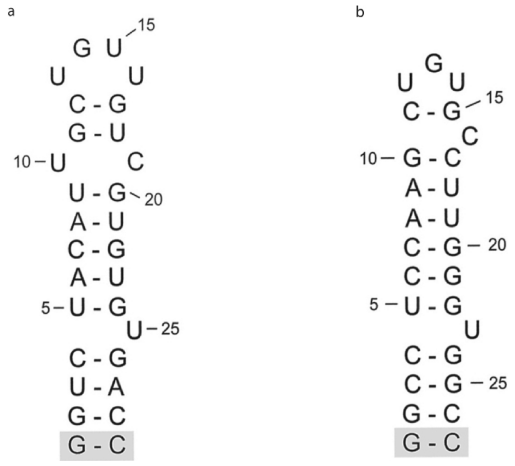

FIGURE 1: Sequence and secondary structure of the apical stem−loop of ε of (a) duck HBV and (b) human HBV. The gray-boxed residues represent structurally silent mutations from the wild type to aid expression.

binding and/or priming. On the basis of these biochemical studies, it has been proposed that the replication initiation is a two-step process, where initial physical binding of the ε apical stem−loop to the RT domain is followed by structural rearrangements in ε, leading up to a priming competent complex in which the ε apical stem−loop is opened (*9*, *13*). The duck UGUU loop, which caps the apical stem, is essential for binding; it contains a U residue, whose mutation abolishes binding (*9*). In contrast, the corresponding loop in human ε is not essential for binding in vitro (*12*) but is required for encapsidation in intact cells (*12*). For heron HBV, the midsection of the apical stem is not base-paired, while in duck HBV, this midsection does contain Watson−Crick base pairs but is interrupted by noncanonical base pairs. The duck (avian) in vitro system data now show that full Watson−Crick base pairing (i.e., stabilization) of this part of the avian apical stem abolishes or greatly weakens RT binding (*9*, *13*). In contrast, the human ε apical stem is fully Watson−Crick base paired, including its midsection, a feature essential for RT binding (*12*). A further interesting difference between the two systems concerns the nonpaired U in the apical stem [U23 in human and U25 in duck (Figure 1)]: in human ε it is required for RT binding, but not in duck (avian). On the other hand, in both systems, the (right) bottom part of the ε apical stem is needed for binding and appears to interact with the RT. In summary, although the overall secondary structures of avian and human ε are quite similar as well as the global build of P and also the overall binding and priming processes, in the sequence and structure requirements differences are apparent.

To improve our understanding of the molecular details of the crucial RT−ε interactions in both avian and human HBVs, we set out to determine the structure, dynamics, and thermodynamic properties of their ε RNAs and domains thereof. Previously, we reported the solution structure and dynamics of the human ε apical stem−loop (*14*−*16*), the thermodynamics of human and avian (duck and heron) apical stem−loops and ε bulges (*17*), and the secondary and loop structure of the duck apical stem−loop (*17*). While secondary structure prediction programs predicted a hexaloop capping the apical stem in human ε, NMR showed formation of a pseudo-triloop (*14*, *15*). The pseudo-triloop is an established motif that consists of a hexaloop with transloop base pairing between residues 1 and 5 and a bulged out residue 6 (*14*, *15*, *18*). The structure of the apical stem of human ε shows that the nonpaired U [U23 (Figure 1)] is partly stacked or resides in the major groove, leading to an angle of ∼20° between the lower and upper part of the apical stem. Here we present the structure of the duck apical stem−loop. Dynamic studies on the human apical stem−loop showed the capping pseudo-triloop to contain highly conserved mobile nucleotides (*16*). Furthermore, thermodynamic studies (UV melting) have shown the human apical stem−loop to be highly stable in contrast to the avian apical stem−loops (*17*). In human HBV, the stability of the middle apical stem is essential for ε−RT binding and ultimately priming (see above), whereas in avian HBV, the instability of the same is essential for RT binding and ultimately priming (see above). The contrasting stabilities of duck (avian) and human ε apical stems are thus each essential for function. Interestingly, while in most avian apical stems, residues in its midsection are not base paired, in wild-type duck the apical stem does contain Watson−Crick base pairs, but they are interrupted by noncanonical base pairs, a U·C base pair flanked by two U·G base pairs (Figure 1). Our NMR imino melting studies on the wild-type duck ε apical stem showed that its midsection, although well formed at lower temperatures, becomes weakened already at 30−40 °C (*17*). The question then arises how such weakening of the apical stem, which is essential for RT binding (see above), affects its structure and dynamics. We therefore conducted NMR relaxation studies on the duck apical stem (−loop) to establish its dynamics on different scales to complement the structural data.

Such a RNA dynamics study is also of biophysical interest, because as far as we are aware, no in-depth dynamics studies have been conducted on an unstable α-helica RNA stem containing noncanonical base pairs, such as that seen in the duck apical stem−loop. RNA dynamics studies by NMR are not as widespread as for proteins as pointed out in recent reviews (*19*−*24*). Dynamics studies of different degrees of comprehensiveness have been conducted on the active site dynamics of the lead-dependent ribozyme (*25*−*27*), the IRES element (*28*, *29*), a tRNA (*30*), two RNAs in their free and protein-bound states (*31*−*33*), a group I intron (*34*), and conformational exchange in an RNA with a nonpaired U residue in its helical stem (*35*). Schwalbe et al. studied in depth the dynamics of the UUCG (*36*) and YNMG tetraloops (*37*). Al-Hashimi et al. introduced the concept of helix elongation to derive domain motion from NMR spin relaxation and/or RDC data (*19*, *38*, *39*). Closest to the duck apical stem comes the RNA thermometer studied by Chowdbury et al. (*40*), which has a network of weak hydrogen bonds within a helix. With the onset of heat shock at 42 °C, destabilization of the RNA structure starts in this region (*40*). The weakened middle section of the duck apical stem also "melts" already at slightly elevated temperatures (30−40 °C) (*17*). Chowdbury et al. (*40*) presented the structure of this RNA thermometer and investigated its base pair opening by imino exchange but did not conduct an NMR dynamics study. A dynamics study of the unstable duck ε apical stem−loop and comparison with the stable human counterpart will thus provide new biophysical data on how decreased RNA stem stability may affect dynamics on different time scales.

Furthermore, a dynamics study of the duck apical stem is of interest, because RT binding of the duck apical stem involves a weak secondary structure. This is unusual in light of the recent classification of RNA−target interactions as discussed below. The findings from molecular biology clearly show that conformational changes play a prominent role in the interaction between RT and ε leading up to the primer synthesis (*9*). This

is in line with analyses of available RNA−protein structures and their dynamics in free and bound states, which demonstrated that RNA−target binding most commonly occurs by mechanisms involving conformational changes rather than rigid lock-and-key docking; this dynamic binding occurs not only by the well-known mechanism of "induced fit" but also by a second mechanism, namely "conformational or tertiary capture" (*19*, *38*, *39*, *41*, *42*). The reason for the prominence of these dynamic mechanisms is thought to lie in the hierarchical folding of RNA. In contrast to proteins, secondary structures in RNAs are highly stable whereas tertiary structures are weak. Consequently, helical domains can easily reorient upon target binding (induced fit). This type of binding can be associated with target selectivity that is based on structure, "structural selectivity" (*19*, *42*), and was thought to dominate when a change in conformation in itself is sufficient to activate a biological process. Alternatively, the weak tertiary interactions provide the free RNA with the opportunity to probe a range of different conformations, one or more of which are captured upon binding (conformational or tertiary capture). This mechanism can be associated with "dynamic selectivity" and is thought to occur when the target is required to be present to activate the biological process. In the classification of RNA−target interaction described above, it is assumed that secondary structures in RNAs are highly stable. The duck ε apical stem−loop is, in contrast, unstable, and this instability is essential for binding, suggesting that a different aspect of RNA dynamics is here involved in the interaction. Dynamics studies on the unstable duck ε apical stem−loop and comparison with the stable human counterpart will provide new data and broaden the scope of knowledge on dynamic RNA−protein interaction mechanisms.

In this paper, we present the structure and dynamics of the ε apical stem−loop of duck HBV determined by NMR spectroscopy. The structure is based on NOEs and dihedral distances complemented with a large number of C−H residual dipolar couplings and is thus of high quality. The dynamics at different time scales have been determined by means of NMR relaxation. We compare these structure and dynamics data with those from previous studies on the human apical stem−loop.

MATERIALS AND METHODS

RNA Sample Preparation. RNA samples were prepared as previously described (*17*). For RDC measurements, two ^{13}C, ^{15}N fully labeled samples in a 93:7 H_2O/D_2O mixture with 0.1 mM EDTA and 10 mM sodium phosphate buffer (pH 6.7) and a concentration of 0.72 mM were used. One of the samples was dissolved in 15 mg/mL Pf1 phages (Asla Biotech, Riga, Latvia) for partial alignment to measure C−H residual dipolar couplings (*43*). The isotropic sample was also used for ^{13}C relaxation measurements.

NMR Spectroscopy. NOE and ribose J_{HH} coupling were measured as described previously (*17*, *44*−*46*) and converted to structure restraints as described previously (*15*, *45*−*47*). For RDC measurement, HSQC, sometimes in IPAP mode, and two-dimensional (2D) and three-dimensional (3D) experiments based on HCCH TOCSY were conducted at 15 °C to obtain N−H and C−H couplings (K. A. M. Ampt, M. Tessari, and S. S. Wijmenga, manuscript submitted). NMR data were processed using NMRPipe and analyzed using Sparky (*48*, *49*). Chemical shift assignments have been submitted to the BMRB database as entry 15656 (*44*).

^{13}C Relaxation Measurements. ^{13}C T_1, ^{13}C $T_{1\rho}$, and ^{13}C-[^1H] NOE values were measured for C5, C1′, C2, and C8 nuclei at 15 °C, on a Varian Unity INOVA600 spectrometer operating at a ^1H frequency of 599.91 MHz equipped with a triple-resonance ($^1H/^{13}C/^{15}N$) probe with *XYZ* gradients. All data were recorded in interleaved fashion as a series of 2D (^{13}C, ^1H) spectra using sensitivity-enhanced pulse sequences with pulse field gradients (*50*−*53*). For C5 and C1′, constant time evolution in the indirect dimension was used to prevent peak broadening due to homonuclear ^{13}C coupling. For T_1 and $T_{1\rho}$ experiments, 16 scans per FID were acquired using a recovery delay of 2.5 s. For $^{13}C[^1H]$ NOE experiments, 32 scans per FID were acquired, using a recovery delay of 4.9 s. Every relaxation experiment was performed two to five times to check for the reproducibility of the results. All T_1 data sets consisted of a series of eight 2D spectra with relaxation times between 20 and 800 ms. Similarly, $T_{1\rho}$ data sets consisted of a series of eight 2D spectra with relaxation times between 4 and 32 ms. For C2 and C8, a continuous spin-lock field of ∼4.4 kHz was employed. For C1′ and C5, a lower spin-lock field (1.3 and 2.7 kHz, respectively) was used to minimize Hartmann−Hahn transfer to scalar coupled ^{13}C nuclei (*54*). Peak intensities were used to fit T_1 and $T_{1\rho}$ relaxation data to exponentially decaying functions. $T_{1\rho}$ values were corrected for resonance offset using standard procedures (*36*). The influence of $^{13}C-^{13}C$ interactions on ^{13}C relaxation plays a more significant role with RNA molecules increasing in size. However, as shown previously, the C−C interactions in molecules similar in size to the apical stem−loop studied here play a minor role (*16*, *31*).

Relaxation dispersion experiments on H2 protons were performed on a Varian Unity INOVA600 spectrometer at 35 and 37.5 °C (and on a Varian Unity INOVA spectrometer at 500 MHz and 35 °C) using a standard relaxation-compensated CPMG scheme (*55*, *56*), with a constant time duration of 15 ms (500 MHz) or 20 ms (600 MHz) and a delay between 180° pulses ranging from 268 μs to 7.5 ms. All experiments were conducted in one-dimensional (1D) fashion; for each experiment, 1024 scans were acquired with a recovery delay of 3 s.

Structure Calculations. Structure calculations were conducted with X-PLOR 3.851 using a torsion angle dynamics protocol (*17*). Starting from an extended structure, we generated 500 structures using classical NMR restraints (Table S1 of the Supporting Information). The 20 lowest-energy structures were submitted to a second round of torsion angle dynamics, generating 20 refined structures out of each selected structure. From the resulting 400 refined structures, the 20 with the lowest energy were selected for RDC refinement, all with NOE violations of < 0.5 Å and with dihedral violations of $< 5°$. For each of these starting structures, the rhombicity and the axial component of the alignment tensor were calculated using the method proposed by Wu and co-workers as well as with Module (*57*). Values for D_a of −25 Hz and R of 0.08 were used to calculate five refined structures from each starting structure, resulting in 100 RDC refined structures. Next the stem parts (i.e., residues 1−4, 5−13, 16−24, and 26−29) were refined for their overly large helical rise (i.e., structures with an average helical rise of 3.5 instead of 2.8 were obtained). This was done by rebuilding the helix with a helical rise of 2.80 and X-displacement of −4.40 in 3DNA (*58*) and substituting it in the structure, after which the RDC refinement protocol was run again; no restraint violations occurred during this refinement. The final 10 lowest-energy

structures have been submitted to the RCSB Protein Data Bank (PDB) as entry 2K5Z.

Modelfree Analysis. Modelfree 4.20 was used to analyze ^{13}C spin relaxation parameters T_1, T_2 (calculated from $T_{1\rho}$), and heteronuclear ^{13}C NOE. ^{13}C chemical shift anisotropies were taken from Stueber and Grant (150 ppm for C2, 138 ppm for C5, and 134 ppm for C8) and Duchardt and Schwalbe (45 ppm for C1′) (*36*, *59*). Distances of 1.104 Å for base C−H bonds and 1.115 Å for C1′−H1′ bonds were used (*54*). HydroNMR was used to estimate a value for the rotational correlation time (τ_c) of 9.4 ns (*60*). This correlation time was used in Modelfree (*61*) to determine an axial symmetric diffusion model with a τ_c of 8.6 ns and a diffusion anisotropy of 2.7. Model selection was performed as suggested by Mandel et al., using Occam's razor (*61*). For a few spins, the use of the flowchart of Mandel et al. indicated model 3 (determination of S^2 and R_{ex}) should be used. However, the use of model 3 did not seem accurate since no exchange was found when using this model, and the flowchart was used to determine a more complicated model.

RESULTS

In previous studies, we have performed structure calculations on the UGUU tetraloop (*17*). From these calculations, it was evident that a U·U base pair is formed in the tetraloop, between residues U13 and U16. This is consistent with the presence of H3 of U13 in the imino region of the NMR spectra. Furthermore, the shift to fewer parts per million of the H5/6 resonances of U13/16 (*44*) with respect to reference values (*62*) shows that they experience ring currents, which indicates stacking consistent with base pair formation. H3 of U16 could not be detected in the imino spectrum, most likely due to movement of U15 leaving U16 accessible to solvent. In the stem, we find that the H5/6 resonances of U10 and C19 are shifted to fewer parts per million and thus experience ring current effects. This indicates stacking of these bases and suggests formation of a U10 and C19 noncanonical base pair. In studies conducted on a segmental labeled sample of full ε, we could observe and identify, thanks to the reduction in the level of overlap, the imino resonance of U10 (U28 in full ε) in the NMR imino spectrum (*63*). This provides further evidence for the existence of a U10 and C19 base pair. Sugar puckering modes were derived from observed versus non-observed H1′−H2′ cross-peaks in the $^1H-^1H$ DQF-COSY spectrum, as well as from C1′−H1′ and C2′−H2′ couplings (*17*, *64*). All residues are N-puckered, except for loop residues 14−16, which are S-puckered; for residue 25, no pucker could be established.

Structure. Initial structure calculations were conducted with classical restraints, like NOEs and dihedrals, supplemented with hydrogen bond restraints and weak planarity restraints for base pairs as described below (Table S1 of the Supporting Information; see PDB entry 2K5Z for the full list of restraints used in the calculations). Hydrogen bond restraints were included for canonical base pairs based on experimental evidence, i.e., the presence of imino resonances and their NOEs. For the two noncanonical base pairs (U13·U16 and U10·C19), hydrogen bond restraints were included on the basis of the presence of imino resonances and set as loose restraints between U13 O2 and U16 H3, U13 H3 and U16 O4, U10 O4 and C19 H41, and U10 H3 and C19 N3. For the canonical base pairs and for the noncanonical base pair, U10·C19, weak planarity restraints were included. No planarity restraint was put onto the U13·U16 base pair closing the UGUU tetraloop. Starting from an extended structure, we calculated a set of 400 structures, of which 115 showed no NOE distance and no dihedral angle violations larger than 0.5 Å and 5°, respectively, as described in Materials and Methods. While NOEs and dihedral restraints can provide valuable information about the local structure, it is difficult to obtain information about long distances. It has therefore become increasingly common to include residual dipolar couplings (RDCs) in structure calculations as they provide information over long distances (*20*). Aromatic and sugar CH RDCs as well as imino NH RDCs were determined employing phages as alignment media. Using NOEs and dihedral restraints complemented with a relatively large number (98) of these RDCs, the 20 lowest-energy structures from the initial calculations were refined. RDCs from residues 15 and 16 were not used in the refinement since their narrow and intense resonances suggested that these residues showed local mobility. This was later confirmed by NMR relaxation data (see below). Moreover, their RDC values were small, suggesting averaging out due to internal motion. Indeed, when the RDCs of residues 15 and 16 were included in the calculations, they consistently showed violations. For instance, when the sugar pucker of residue 16 was left undetermined, the sugar RDCs forced it into N-pucker, even though there is clear evidence, from C1′−H1′ and C2′−H2′ *J* couplings, that this residue is S-puckered. An overlay of the 10 lowest-energy structures is shown in Figure 2.

The root-mean-square deviation (rmsd) of the RDC-refined structure set is 0.92 ± 0.43 Å (Table S2 of the Supporting Information). The structure is well-defined and consists of two helical stems and a UGUU tetraloop (for helical parameters, see Table S3 of the Supporting Information). The lower stem is separated by the nonpaired U from the upper stem with a bend angle of 10 ± 3°; the 3° standard deviation represents the uncertainty observed in the 10 lowest-energy structures and does not represent the amplitude of motion. The nonpaired U25, which separates these two stems, is located mostly in the major groove. The upper stem contains a well-structured U·C base pair, of which a detailed top view is show in Figure S1 of the Supporting Information (U10·C19 base pair). The UGUU tetraloop is well-structured with G14 stacked on top of U13. The tetraloop is closed by a U13·U16 base pair, of which a detailed view is shown in Figure S1. Loop residue U15 is sticking out of the structure. From the structure calculations, a preference for a specific position (straight up, in the minor or major groove) of U15 could not be established. Indeed, dynamics studies (see below) indicate this residue to be mobile, and it, most likely, does not have a specific static position. It is therefore highly solvent accessible, in agreement with the absence of the imino resonance in the H_2O imino spectrum (*17*).

Dynamics Studies. The previously described melting studies gave an indication of the dynamics of the duck apical stem−loop on the millisecond to second time scale (*17*). Residual dipolar couplings can give an indication of dynamics on the pico- to millisecond time scale, while relaxation measurements can indicate dynamics on the pico- to nanosecond time scale. The relatively small RDCs of residues 15 and 16 already indicated that these residues are mobile. To further investigate dynamics on a fast time scale, relaxation studies, T_1, $T_{1\rho}$, and NOE measurements, were conducted for C2, C8, C5, and C1′ (Materials and Methods).

In Figure 3, the $T_{1\rho}$ relaxation times for the C1′−H1′, C2−H2, C5−H5, and C8−H8 resonances are presented. The average $T_{1\rho}$ value for the C1′−H1′ resonance is 29.6 ms, excluding terminal residues and loop residues. For the C2−H2, C5−H5, and

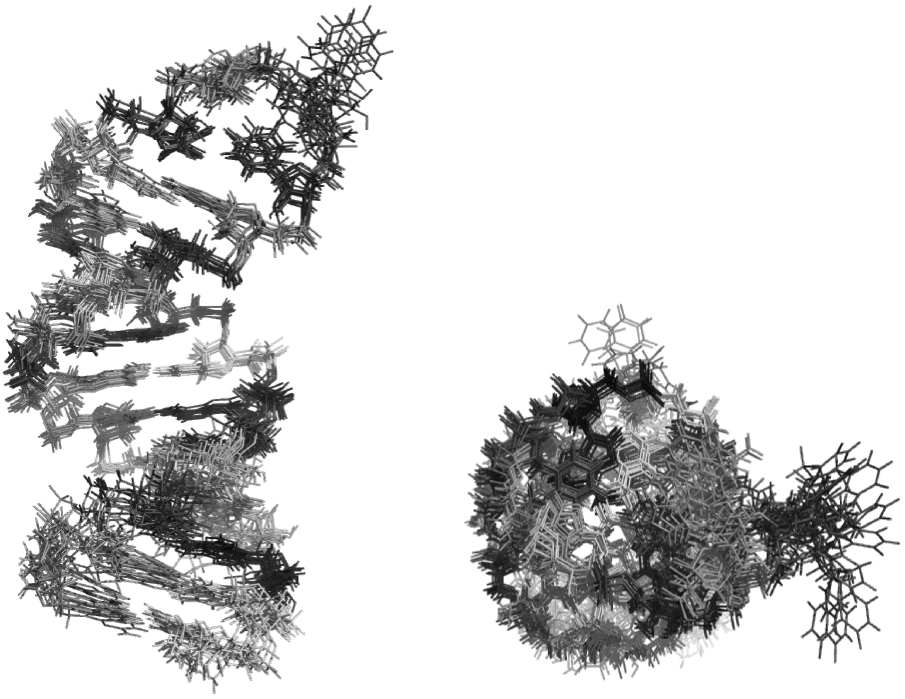

FIGURE 2: Overlay of the 10 lowest-energy structures of the duck HBV ε apical stem−-loop after RDC refinement (PDB entry 2K5Z).

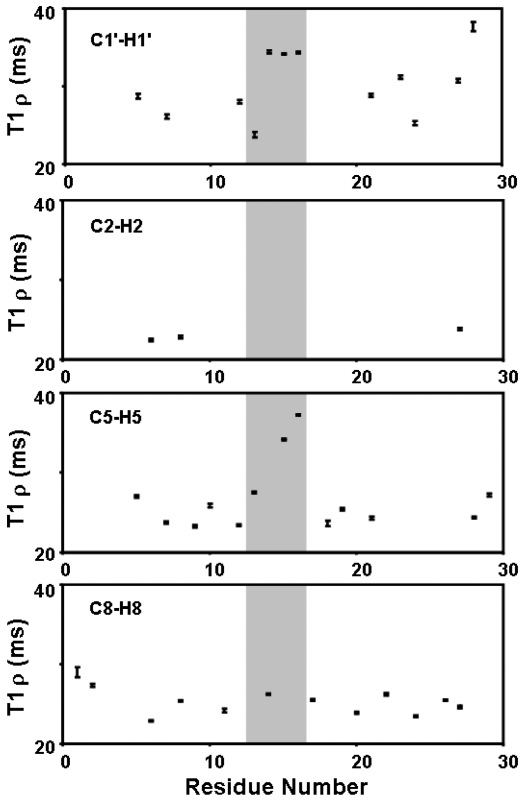

FIGURE 3: ^{13}C $T_{1\rho}$ relaxation times for C1′, C2, C5, and C8. Resonances that were partially or completely overlapped were excluded from the analysis. Each data point is the average of two to five separate measurements. The average percentage error is 1%, based on replicate measurements. The individual errors are indicated as error bars. The gray box indicates the tetraloop.

C8−H8 resonances, the average $T_{1\rho}$ values, again excluding terminal and loop residues, are 23.0, 24.3, and 24.7 ms, respectively. Thus, the $T_{1\rho}$ values for the ribose units are on average larger than those for bases, indicating a somewhat higher mobility in the ribose units than in the base units. It has to be noted that in the ribose unit, due to overlap, $T_{1\rho}$ values other than those for the C1′−H1′ cross-peak were not determined. Loop residues U15 and U16 have ribose $T_{1\rho}$ values that are 15% larger than the average values, while their base $T_{1\rho}$ values are increased by 150%, indicating that these residues are more flexible on the pico- to nanosecond time scale than the other residues. It also suggests that this additional mobility is mostly expressed in their base units. Loop residue G14 has a ribose $T_{1\rho}$ that is 15% larger than the average, while its base $T_{1\rho}$ is similar to the average value. Loop residue U13 has $T_{1\rho}$ values similar to the average values. Shajani and Varani investigated the dynamics of *Hha*I target DNA and noted that the C1′−H1′ resonances of the pyrimidines, especially in the case of deoxycytidines, had a larger transverse relaxation time than the purines (*65*). Dynamics studies of the DNA dodecamer d(CGCGAATTCGCG)$_2$ also revealed that the C1′−H1′ resonances of the nonterminal deoxycytidines had an increased transverse relaxation time (*66*). In our RNA relaxation data, there is no such distinction observed. In fact, the C1′−H1′ resonances of the cytosine residues have, on average, the same relaxation time as the C1′−H1′ resonances of the other residues. The same observation can be made from relaxation data of the human apical stem−loop (*16*). This suggests that mobility patterns are different in A-helices (RNA) versus B-helices (DNA).

Further analysis was conducted using Modelfree (*61*). The analysis resulted in a correlation time of 8.6 ns and a diffusion anisotropy of 2.7. This agrees reasonably well (within 9%) with a correlation time of 9.4 ns and a diffusion anisotropy of 2.4, respectively, predicted with HydroNMR (*60*) given the structures derived by RDCs. Full Modelfree results are given in Table S4 of the Supporting Information, while Figure 4 shows the order parameter, S^2, as a function of nucleotide sequence.

The analysis shows that the stem nucleotides are rigid in the base moieties with S^2 values of 0.86 ± 0.06. The ribose moieties in the stems show slightly more motion with S^2 values of 0.80 ± 0.10. These are usual values (*16*, *36*, *54*). The time scale of the

motions is on average 700 ps. The residues around the nonpaired U25, i.e., the opposite residue U5 and the neighboring residue G24, show movement on a slower scale (on average 1000 ps). The loop residues, U13, G14, U15, and U16, can be divided into two sets. U13 and G14 have S^2 values similar to those of the stem residues, while U15 and U16 exhibit high mobility for both the base and ribose moieties.

To further investigate the dynamics, relaxation dispersion experiments were conducted on H2 spins (see Figure 5 and Figure S3 of the Supporting Information). These experiments monitor the presence or absence of conformational exchange on the micro- to millisecond time scale and, in this case, in the lower stem (A27) and in the middle of the upper stem (A6 and A8). For the sake of comparison with previous imino melting studies, the experiments were conducted at 35 and 37.5 °C (*17*). The difference between the 1D NMR spectra from the dispersion at high (1400 Hz) and low (100 Hz) effective CPMG fields (Figure 5) shows that residues A6 and A8 in the middle part of the upper stem undergo exchange at these temperatures. No conformational exchange is observed for residue A27 in the lower stem. The full relaxation dispersion curves measured at 500 and 600 MHz at 35 °C and shown in Figure S3 of the Supporting Information for 500 MHz display the same features, namely, exchange for H2 of A6 and A8, but not for H2 of A27. The exchange dispersion curves of H2 of A6/8 are characterized by following fit parameters: p_b = 0.024, k_{ex} = 506 s^{-1}, R_2^0 = 21.5 s^{-1}, and $\Delta\omega$ = 1651 rad s^{-1} (=0.53 ppm) for 500 MHz; p_b = 0.045, k_{ex} = 645 s^{-1}, and $\Delta\omega$ = 2209 rad s^{-1} (=0.59 ppm) for 600 MHz. The parameters are fully defined in the legend of Figure S3. Thus, the H2 atoms of A6 and A8 exchange with a rate (k_{ex}) of 506−645 s^{-1} (lifetime of 1.6−2 ms) to a state that is populated to a degree of only 2.4−4.5%. It could further be established that A6 and A8 each exchange with a state in which their H2 resonates at a higher chemical shift, i.e., a state in which their H2 experiences less current and thus their bases are less stacked. Thus, A6 and A8 exchange most likely with an unstacked/unfolded state. Note that the $\Delta\omega$ derived from the relaxation dispersion curves has a value of ca. 0.6 ppm, so that in the low-populated (2.4−4.5%) state, the H2 atom of A6/A8 would resonate at ca. 8.1 ppm. In other words, H2 is then in a semi-unstacked state, because in the fully stacked state H2 resonates at 7.5 ppm, while the H2 reference value is 8.4 ppm, which corresponds to a conformation in which it does not experience any ring currents, while an unfolded state would experience some weak ring current effects (ca. 8.0−8.2 ppm).

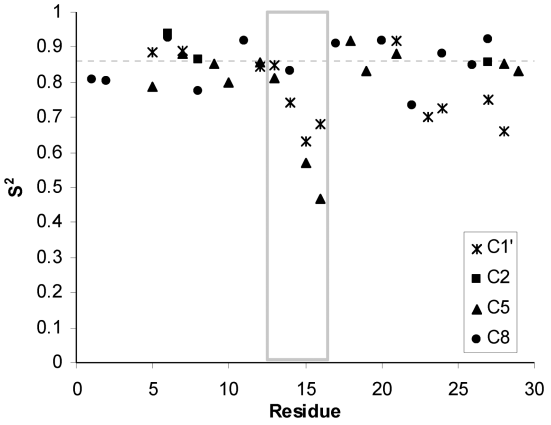

FIGURE 4: ^{13}C S^2 parameters (see also Table S4 of the Supporting Information) as a function of nucleotide sequence. Crosses represent data for C1′ atoms, squares data for C2 atoms, triangles data for C5 atoms, and circles data for C8 atoms. The dashed line represents the average S^2 value of the stem base CH groups. A gray box surrounds the data for the loop residues.

DISCUSSION

The structure of the apical stem−loop of ε duck HBV has been derived from NOEs and *J* coupling data complemented with long distance information contained in N−H and C−H RDCs. A large number of RDCs (~100) have been used in the final calculations, so that a set of high-quality and well-defined structures is obtained, in which not only local structure features but also long-range features are correct. In addition, this large number of RDCs provides complementary insight into the internal dynamics, which was further assessed on the basis of NMR relaxation data.

The structure set shows the main features of the apical stem−loop. The stem can be divided into two parts, the lower stem, which is separated from the upper stem by a nonpaired U (U25), and is capped by a UGUU tetraloop. The tetraloop is closed by a U·U base pair [U13·U16 (see Figure S1 of the

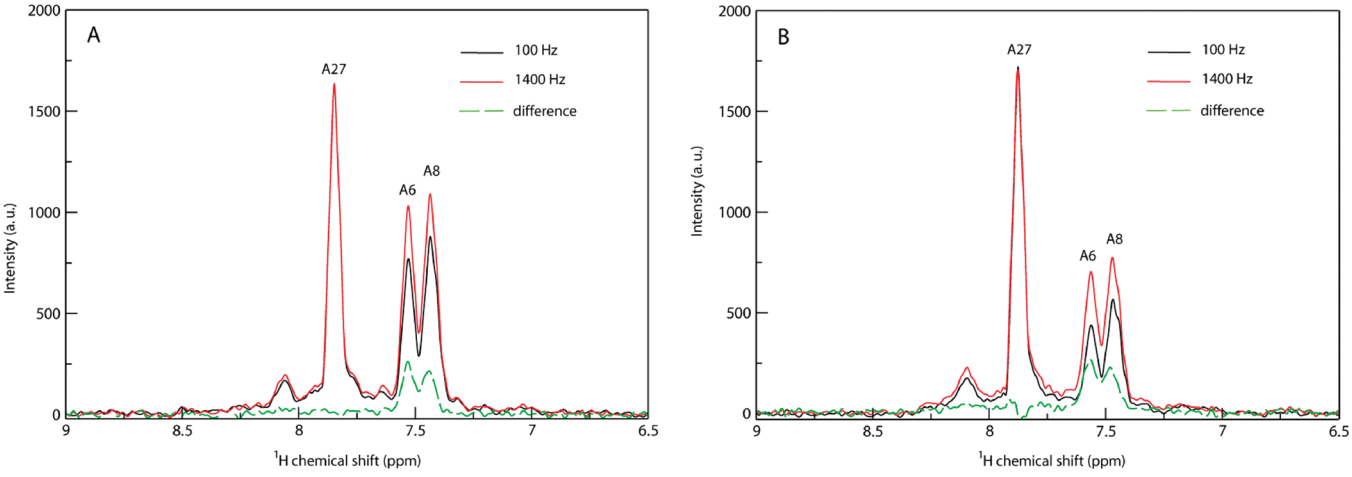

FIGURE 5: NMR 1D slices from the H2 relaxation dispersion experiments of the 0.72 mM apical stem−loop of duck HBV fully labeled with ^{13}C and ^{15}N [10 mM sodium phosphate (pH 6.7), 0.1 mM EDTA, and a 93:7 H_2O/D_2O mixture]. The slices are measured at high (1400 Hz, minimal exchange) and low (100 Hz, maximum exchange) effective CPMG field strengths at 35 °C (A) and 37.5 °C (B), respectively. A difference (dashed curve) between high and low field indicates directly that the proton experiences conformational exchange, here A6 and A8.

Supporting Information for a detailed view)]. The bend angle between the two helical stems was determined to be 10 ± 3°, which is comparable to the bend angle of ca. 20°, seen in the structure of the apical stem−loop of human HBV. In the calculated structures, the nonpaired U25 is located mostly in the major groove. At 25 °C, no resonances could be derived for U25, apart from those of H5 and H6, which were assigned by elimination of all other H5−H6 correlations in the DQF-COSY spectrum. The absence of NOE cross-peaks between these resonances and other resonances suggests U25 is not stacked, at least not all the time. In the $^{13}C-^{1}H$ HSQC spectrum, no H5−C5 or H6−C6 correlations were detected for U25, suggesting broadening of the C5 (and possibly C6) resonances. Furthermore, at 15 °C these chemical shifts of U25 were not detected in the HSQC spectrum and well-resolved 2D and 3D HCN type base−ribose correlation experiments (*44*). It appears therefore highly likely that all or some of the U25 resonances are broadened beyond detection, due to motional averaging on an intermediate time scale. Finally, we note that in the upper stem a U10·C19 noncanonical base pair is formed (see Figure S1 for a detailed view), flanked by two G·U base pairs.

The NMR relaxation data provide a view of the dynamics of the apical stem−loop. As far as we are aware, this is the first NMR dynamics study of an RNA molecule with an unstable secondary structure. Most stem residues undergo only slight motion on the pico- to nanosecond time scale, i.e., $S^2 = 0.86$, which corresponds to a C−H fluctuation within a cone with an opening half-angle of ∼20°. The time scale of the fluctuations appears to be subnanosecond (∼700 ps), except for residues neighboring or opposite the nonpaired U (U25) and residues neighboring the U10·C19 base pair, which have a somewhat higher degree of fluctuation on a time scale of ∼1 ns. The S^2 values and time scales are similar to those commonly found in stable RNA secondary structures (see, e.g., ref *16*). In the UGUU tetraloop, the solvent-exposed U15 is quite flexible ($S^2 \sim 0.6$), while U16 in the U13·U16 base pair also shows enhanced motion. In addition, the RDCs of U16 and U15 could not be fitted in the structure calculation, further confirming their dynamic nature. The other tetraloop residues have S^2 values similar to those of the stem residues. It appears therefore that, apart from these dynamic residues, the apical stem−loop is quite rigid at 15 °C on the pico- to nanosecond time scale.

Previously, we found that the apical stem−loop of duck ε is unstable and partially "melts" at a temperature as low as 35−40 °C, which is evident form UV melting studies (*17*). In the apical stem−loop, a nonpaired U residue (U25) separates the lower and upper stem. The latter contains a number of noncanonical base pairs. NMR temperature studies showed disappearance, at a temperature as low as 35−40 °C, of imino resonances from residues in the middle part of the upper stem, but not from residues in the lower stem or directly under the tetraloop, suggesting "melting" of the middle part of the upper stem. It might therefore be hypothesized that such an unstable stem would exhibit increased dynamics. However, we do not observe in our NMR relaxation studies abnormally high internal dynamics in the upper stem on the pico- to nanosecond time scale. To further investigate how the instabilities affect dynamics, a temperature profile ranging from 15 to ∼40 °C has been measured of the chemical shifts of H2 and H8 (Figure S2 of the Supporting Information). For H8, no specifically different behavior is seen for the residues in the middle part of the upper stem, apart from G11 next to the U10·C19 base pair and G24/G26 next to the nonpaired U25 (as well as G14 in the loop). While H2 of A27 in the lower stem shows no change in chemical shift, a small but significant change in the chemical shift toward a higher number of parts per million is observed for H2 of A6 and A8 in the middle part of the upper stem. This indicates an increased level of nonstacked open states at higher temperatures. Note that conformational shifts of H2 are larger than of H8, so that small structural changes are more readily evident in H2 chemical shifts than H8 chemical shifts. To confirm the presence of conformational exchange on the micro- to millisecond time scale at higher temperatures, relaxation dispersion curves for H2 (C2) have been measured at 35 and 37.5 °C (1D slices of two points on the curve are presented in Figure 5, and relaxation dispersion curves are shown in Figure S3 of the Supporting Information). We indeed find that residue A27 in the lower stem shows no conformational exchange (see Figure 5 and Figure S3). On the other hand, residues A6 and A8 in the middle of the upper stem do show conformational exchange to a state in which H2 resonates at a higher number of parts per million, consistent with it being an open state. The origin of the instabilities, most apparent in the middle part of the upper stem, lies therefore in enhanced conformational exchange to a semi-unstacked state on the millisecond time scale, a time scale corresponding to that of base pair opening. Moreover, previous studies have demonstrated that these same residues exhibit an increased level of imino exchange and thus an increased level of base pair opening. It appears therefore appropriate to attribute the enhanced exchange to base pair opening. Surprisingly, no enhanced dynamics on the pico- to nanosecond time scales is seen in the unstable upper stem.

How can the structure and dynamics of the free apical stem−loop of duck ε provide insight into its binding to the viral RT, an event essential for viral replication? The binding of ε to RT appears to be a two-step process, in which initial physical binding is followed by major conformational changes that lead to a priming competent complex, in which the apical stem−loop of ε has opened up (*3*, *5*, *9*, *12*). All these events, the initial physical binding and subsequent rearrangements of ε, appear to take place in the palm of the hand of the RT domain. Previously, we reported on the structure (*14*, *15*) and dynamics (*16*) of the apical stem−loop of human HBV ε. A comparison of the structure and dynamics of the ε apical stem−loops of duck HBV, reported here, and human HBV can now be made and may provide further insight into the ε−RT interaction. We also discuss how this ε−RT interaction may fit the well-known and recently proposed classes for RNA target interactions.

In a comparison of the human and duck ε apical stem−loops, several similarities are seen, but differences do stand out. The overall shapes are highly similar. Both have a nonpaired U [U25, duck; U23, human (Figure 1)], separating the lower and middle/upper parts of the stem. The presence and similar position of the nonpaired U lead to a kink in the helix axis in the same direction and of a similar magnitude (bent angles of 10 ± 3° and 20 ± 5° in duck and human ε, respectively). The loops capping the ε apical stem−loops are different; in the human form, a well-formed pseudo-triloop is seen, and in the duck (avian) form, a well-formed UGUU tetraloop is seen. With regard to dynamics, we find in both systems relatively high order parameters ($S^2 \sim 0.9$ on average) of the C−H vectors of residues in the lower and upper/middle stem, indicating that the whole kinked apical stem−loop forms in both systems a mainly rigid unit on short time scales. The conservation of the slightly kinked helical shape between human and duck apical stem−loops suggests its importance for

the interaction with the RT; e.g., it may be required for the apical stem−loop to fit into the palm of the RT. A major difference between the two systems is, that in contrast to the human form, the duck apical stem−loop is unstable, mostly in the middle part of the upper stem. This instability enhances conformation exchange involving base pair opening for residues in the middle part of the upper stem as evidenced by our NMR data but does not affect dynamics on the pico- to nanosecond time scales. From our NMR data, we can thus conclude that in duck ε open base pair states are present in the middle part of the upper stem, although their population is likely to be low. The ε−RT binding in avian HBV requires weak or absent base pairing in the middle of the ε apical stem−loops; i.e., stabilization of this part of the stem abolishes or greatly weakens binding (*9*). Together, this indicates that these open states and thus dynamics form an intrinsic part of the initial binding to RT for the duck (avian) systems. In view of these characteristics, it is interesting to consider the known classes of RNA target interaction in which the ε−RT binding in duck and human can be categorized.

It has recently been proposed and established that in addition to the well-known class of induced fit, a second mechanism, conformational or tertiary capture, often governs RNA−target interaction(*19*, *38*, *39*, *42*). The reason for the prominence of these dynamic interaction mechanisms in RNAs is thought to originate from their usually highly stable secondary structures (helices) and weak tertiary structures. Consequently, helical domains can easily reorient upon target binding (induced fit) or probe a range of different conformations in the free RNA, one or more of which are captured upon binding (conformation or tertiary capture). The underlying assumption is thus that RNAs (usually) have stable secondary structures. Indeed, the examples discussed all concern RNAs with stable secondary structures. However, the duck ε apical stem−loop has, in contrast, an unstable secondary structure, and this instability is essential for RT binding (*3*, *5*, *9*, *12*) (see also below). This indicates that in the ε−RT interaction an aspect of RNA dynamics different from that previously proposed is involved, namely one involving a weak secondary structure instead of or together with a weak tertiary structure. As described and discussed above, from relaxation dispersion and other NMR evidence, one can conclude that the instability leads to enhanced conformational exchange on the millisecond time scale to an open state, which can be attributed to a base pair open state. Consequently, the duck ε−RT binding takes place thanks to enhanced dynamics within an unstable secondary structure element, specifically thanks to enhanced conformational exchange to base pair open states as discussed above, e.g., by capture of bases in the base pair open states.

Note that no base-specific interactions appear to be required for effective duck ε−RT binding as follows from, for example, the lines of evidence given below (*3*, *5*, *9*, *12*). (1) During the SELEX experiments, no single winning sequence emerged. (2) From several rounds of SELEX, mutants with a high C content emerged that still were good binders; the high C content precludes base pairing. Therefore, a specific sequence is unnecessary for binding in these regions (*3*, *5*, *9*, *12*). Instead, base pairing that leads to stabilization of the middle part of the upper stem of duck ε abrogates ε−RT binding.

Although base pair open states are essential for binding, the possibility that the slightly kinked shape of the apical stem−loop aids in the RT interaction cannot be excluded. Further, the tetraloop capping the duck (or avian) ε apical stem is also essential for RT binding and appears to interact with the RT through a loop residue (U15) since its mutation abrogates binding (*9*, *13*). This residue is highly mobile and could thus be considered to interact through a conformational capture mechanism. In summary, the unstable secondary structure of the ε apical stem−loop makes duck ε−RT binding unusual in light of recent classifications of RNA target interactions that assume stable secondary structures. The binding requires exchange with base pair open states and probably occurs by capture of bases in these open states. Tertiary capture and conformational capture are used interchangeably in literature, because it is assumed that RNA secondary structures are highly stable. However, in view of our findings, we suggest that a distinction between the two should be made. The mechanism for duck ε−RT binding, in which a weak secondary structure is important for binding, could then be identified as a "secondary conformational capture" mechanism, in contrast to the more common tertiary capture, in which a weak tertiary structure is important for binding.

In contrast to the duck form, the apical stem−loop of human ε is highly stable (*15*, *17*). As pointed out above, the human ε−RT binding is likely to occur by fitting the kinked shape of the apical stem−loop into the palm of the RT. The mechanism could be likened to that of induced fit and/or tertiary capture. The nonpaired residue U23 (Figure 1b) appears to partially insert into the stack of the stem or reside in the major groove, thus inducing small-scale relative motions of the lower versus upper stem (*15*, *16*). Although U23 does show enhanced dynamics on the pico- to nanosecond time scales (*16*), the time scale for partial stacking must be slower than the pico- to nanosecond scale and lies probably in the micro- to millisecond range, although no significant exchange broadening was seen for the U23 resonances of the human ε apical stem−loop. On the other hand, we do appear to observe in the duck ε apical stem−loop exchange broadening for the nonpaired U25 (see above).

After initial binding, the apical stem−loop of ε needs to open up (in human) or to further open (in duck) to form a primer synthesis competent complex (*5*, *9*, *12*). The high stability of the human ε apical stem−loop represents a significant barrier for opening of the stem. The free energy to overcome this barrier may come from the interaction with the RT, but also from interaction of the capping pseudo-triloop with capsid proteins. The pseudo-triloop is not needed for binding in vitro (*12*) but is essential for pgRNA encapsidation and initiation of replication in intact cells (*5*, *12*); furthermore, pseudo-triloops are known to be involved often in interaction with viral capsid proteins (*18*).

CONCLUSION

The structure determination and the dynamics studies by NMR of the duck ε apical stem−loop described here indicate that while its structure is similar to that of its human counterpart, its dynamics are not. The mobility of the structure occurs on different time scales. High mobility on the pico- to nanosecond time scales is observed for two residues of the capping UGUU tetraloop comparable to the one highly mobile residue in the capping pseudo-triloop in the human form. Remarkably, the unstable middle part of the duck ε apical stem−loop displays no enhanced dynamics on the pico- to nanosecond time scales; instead, it exhibits enhanced conformational exchange on the millisecond time scale involving base pair opening. No such conformational exchange is indicated in the stable apical stem−loop of human ε. As far as we are aware, this is the first NMR dynamics study of an RNA molecule with an unstable secondary structure. Stabilization of the duck ε apical stem−loop

is known to abolish binding to RT. Dynamics involving the base pair opening in the unstable part of the apical stem−loop is therefore essential for binding to RT. We hypothesize that initial duck ε−RT binding involves conformational capture of (a) bases in their base pair open states and (b) mobile loop residues. The unstable secondary structure of the ε apical stem−loop makes duck ε−RT binding unusual in light of recent classifications of RNA target interactions that assume stable secondary structures. In contrast, initial binding of the highly stable human ε to RT likely involves fitting of the stable and kinked apical stem−loop into the palm of the hand of the RT by induced fit or conformational or tertiary capture, each a mechanism proposed to commonly govern RNA target interactions. To confirm our model, it would be useful to study the structure of the bound state. Further insight into the ε−RT interaction is also expected to come from the structure and dynamics of the full 60 nt duck and human ε elements, on which work is to be presented soon.

SUPPORTING INFORMATION AVAILABLE

Tables with the number of constraints used in the structure calculations, the structural statistics, helical parameters, and relaxation parameters and a figure of the chemical shift changes at different temperatures. This material is available free of charge via the Internet at http://pubs.acs.org.

REFERENCES

1. Lee, W. M. (1997) Medical progress: Hepatitis B virus infection. *N. Engl. J. Med. 337*, 1733–1745.
2. Ganem, D., and Schneider, R. (2001) Fields Virology , Lippincott, Williams & Wilkins, Philadelphia.
3. Nassal, M. (2008) Hepatitis B viruses: Reverse transciption a different way. *Virus Res. 134*, 235–249.
4. Nassal, M. (2000) DNA Virus Replication , Vol. 26, Oxford University Press, Oxford, U.K.
5. Beck, J., and Nassal, M. (2007) Hepatitis B virus replication. *World J. Gastroenterol. 13*, 48–64.
6. Beck, J., Bartos, H., and Nassal, M. (1997) Experimental confirmation of a hepatitis B virus (HBV) ε-like bulge-and-loop structure in avian HBV RNA encapsidation signals. *Virology 227*, 500–504.
7. Beck, J., and Nassal, M. (2001) Reconstitution of a functional duck hepatitis B virus replication initiation complex from separate reverse transcriptase domains expressed in *Escherichia coli*. *J. Virol. 75*, 7410–7419.
8. Hu, J. M., and Anselmo, D. (2000) In vitro reconstitution of a functional duck hepatitis B virus reverse transcriptase: Posttranslational activation by Hsp90. *J. Virol. 74*, 11447–11455.
9. Hu, K. H., Beck, J., and Nassal, M. (2004) SELEX-derived aptamers of the duck hepatitis B virus RNA encapsidation signal distinguish critical and non-critical residues for productive initiation of reverse transcription. *Nucleic Acids Res. 32*, 4377–4389.
10. Lin, L., Wan, F., and Hu, J. M. (2008) Functional and Structural Dynamics of Hepadnavirus Reverse Transcriptase during Protein-Primed Initiation of Reverse Transcription: Effects of Metal Ions. *J. Virol. 82*, 5703–5714.
11. Hu, J. M., Flores, D., Toft, D., Wang, X. T., and Nguyen, D. (2004) Requirement of heat shock protein 90 for human hepatitis B virus reverse transcriptase function. *J. Virol. 78*, 13122–13131.
12. Hu, J. M., and Boyer, M. (2006) Hepatitis B virus reverse transcriptase and ε RNA sequences required for specific interaction in vitro. *J. Virol. 80*, 2141–2150.
13. Beck, J., and Nassal, M. (1998) Formation of a functional hepatitis B virus replication initiation complex involves a major structural alteration in the RNA template. *Mol. Cell. Biol. 18*, 6265–6272.
14. Flodell, S., Schleucher, J., Cromsigt, J., Ippel, H., Kidd-Ljunggren, K., and Wijmenga, S. (2002) The apical stem-loop of the hepatitis B virus encapsidation signal folds into a stable tri-loop with two underlying pyrimidine bulges. *Nucleic Acids Res. 30*, 4803–4811.
15. Flodell, S., Petersen, M., Girard, F., Zdunek, J., Kidd-Ljunggren, K., Schleucher, J., and Wijmenga, S. (2006) Solution structure of the apical stem-loop of the human hepatitis B virus encapsidation signal. *Nucleic Acids Res. 34*, 4449–4457.
16. Petzold, K., Duchardt, E., Flodell, S., Larsson, G., Kidd-Ljunggren, K., Wijmenga, S., and Schleucher, J. (2007) Conserved nucleotides in an RNA essential for hepatitis B virus replication show distinct mobility patterns. *Nucleic Acids Res. 35*, 6854–6861.
17. Girard, F. C., Ottink, O. M., Ampt, K. A. M., Tessari, M., and Wijmenga, S. S. (2007) Thermodynamics and NMR studies on Duck, Heron and Human HBV encapsidation signals. *Nucleic Acids Res. 35*, 2800–2811.
18. Haasnoot, P. C. J., Brederode, F. T., Olsthoorn, R. C. L., and Bol, J. F. (2000) A conserved hairpin structure in Alfamovirus and Bromovirus subgenomic promoters is required for efficient RNA synthesis in vitro. *RNA 6*, 708–716.
19. Al-Hashimi, H. M. (2005) Dynamics-based amplification of RNA function and its characterization by using NMR spectroscopy. *ChemBioChem 6*, 1506–1519.
20. Latham, M. R., Brown, D. J., McCallum, S. A., and Pardi, A. (2005) NMR methods for studying the structure and dynamics of RNA. *ChemBioChem 6*, 1492–1505.
21. Hall, K. B. (2008) RNA in motion. *Curr. Opin. Chem. Biol. 12*, 612–618.
22. Shajani, Z., and Varani, G. (2007) NMR studies of dynamics in RNA and DNA by C-13 relaxation. *Biopolymers 86*, 348–359.
23. Al-Hashimi, H. M. (2007) Beyond static structures of RNA by NMR: Folding, refolding, and dynamics at atomic resolution. *Biopolymers 86*, 345–347.
24. Getz, M., Sun, X. Y., Casiano-Negroni, A., Zhang, Q., and Al-Hashimi, H. M. (2007) NMR studies of RNA dynamics and structural plasticity using NMR residual dipolar couplings. *Biopolymers 86*, 384–402.
25. Lee, J. H., and Pardi, A. (2007) Thermodynamics and kinetics for base-pair opening in the P1 duplex of the *Tetrahymena* group I ribozyme. *Nucleic Acids Res. 35*, 2965–2974.
26. Hoogstraten, C. G., Wank, J. R., and Pardi, A. (2000) Active site dynamics in the lead-dependent ribozyme. *Biochemistry 39*, 9951–9958.
27. Legault, P., Hoogstraten, C. G., Metlitzky, E., and Pardi, A. (1998) Order, dynamics and metal-binding in the lead-dependent ribozyme. *J. Mol. Biol. 284*, 325–335.
28. Addess, K. J., Basilion, J. P., Klausner, R. D., Rouault, T. A., and Pardi, A. (1997) Structure and dynamics of the iron responsive element RNA: Implications for binding of the RNA by iron regulatory binding proteins. *J. Mol. Biol. 274*, 72–83.
29. Showalter, S. A., Baker, N. A., Tang, C. G., and Hall, K. (2005) Iron responsive element RNA flexibility described by NMR and isotropic reorientational eigenmode dynamics. *J. Biomol. NMR 32*, 179–193.
30. Vermeulen, A., McCallum, S. A., and Pardi, A. (2005) Comparison of the global structure and dynamics of native and unmodified tRNA. *Biochemistry 44*, 6024–6033.
31. Shajani, Z., and Varani, G. (2005) C-13 NMR relaxation studies of RNA base and ribose nuclei reveal a complex pattern of motions in the RNA binding site for human U1A protein. *J. Mol. Biol. 349*, 699–715.
32. Shajani, Z., Drobny, G., and Varani, G. (2007) Binding of U1A protein changes RNA dynamics as observed by C-13 NMR relaxation studies. *Biochemistry 46*, 5875–5883.
33. Oberstrass, F. C., Allain, F. H. T., and Ravindranathan, S. (2008) Changes in dynamics of SRE-RNA on binding to the VTS1p-SAM domain studied by C-13 NMR relaxation. *J. Am. Chem. Soc. 130*, 12007–12020.
34. Eldho, N. V., and Dayie, K. T. (2007) Internal bulge and tetraloop of the catalytic domain 5 of a group II intron ribozyme are flexible: Implications for catalysis. *J. Mol. Biol. 365*, 930–944.
35. Blad, H., Reiter, N. J., Abildgaard, F., Markley, J. L., and Butcher, S. E. (2005) Dynamics and metal ion binding in the U6 RNA intramolecular stem-loop as analyzed by NMR. *J. Mol. Biol. 353*, 540–555.
36. Duchardt, E., and Schwalbe, H. (2005) Residue specific ribose and nucleobase dynamics of the cUUCGg RNA tetraloop motif by NMR C-13 relaxation. *J. Biomol. NMR 32*, 295–308.
37. Ferner, J., Villa, A., Duchardt, E., Widjajakusuma, E., Wohnert, J., Stock, G., and Schwalbe, H. (2008) NMR and MD studies of the temperature-dependent dynamics of RNA YNMG-tetraloops. *Nucleic Acids Res. 36*, 1928–1940.
38. Zhang, Q., Sun, X. Y., Watt, E. D., and Al-Hashimi, H. M. (2006) Resolving the motional modes that code for RNA adaptation. *Science 311*, 653–656.
39. Zhang, Q., Stelzer, A. C., Fisher, C. K., and Al-Hashimi, H. M. (2007) Visualizing spatially correlated dynamics that directs RNA conformational transitions. *Nature 450*, 1263–1267.
40. Chowdhury, S., Maris, C., Allain, F. H. T., and Narberhaus, F. (2006) Molecular basis for temperature sensing by an RNA thermometer. *EMBO J. 25*, 2487–2497.

41. Williamson, J. R. (2000) Induced fit in RNA-protein recognition. *Nat. Struct. Biol. 7*, 834–837.
42. Leulliot, N., and Varani, G. (2001) Current topics in RNA-protein recognition: Control of specificity and biological function through induced fit and conformational capture. *Biochemistry 40*, 7947–7956.
43. Hansen, M. R., Mueller, L., and Pardi, A. (1998) Tunable alignment of macromolecules by filamentous phage yields dipolar coupling interactions. *Nat. Struct. Biol. 5*, 1065–1074.
44. Ampt, K. A. M., Ottink, O. M., Girard, F. C., Nelissen, F., Tessari, M., and Wijmenga, S. S. (2008) ^{1}H, ^{13}C and ^{15}N NMR assignments of Duck HBV apical stem loop of the epsilon encapsidation signal. *Biomol. NMR Assignments 2*, 159–162.
45. Cromsigt, J., van Buuren, B., Schleucher, J., and Wijmenga, S. (2001) Resonance assignment and structure determination for RNA. *Methods Enzymol. 338*, 371–399.
46. Wijmenga, S. S., and van Buuren, B. N. M. (1998) The use of NMR methods for conformational studies of nucleic acids. *Prog. Nucl. Magn. Reson. Spectrosc. 32*, 287–387.
47. Wu, B., Girard, F., van Buuren, B., Schleucher, J., Tessari, M., and Wijmenga, S. (2004) Global structure of a DNA three-way junction by solution NMR: Towards prediction of ^{3}H fold. *Nucleic Acids Res. 32*, 3228–3239.
48. Delaglio, F., Grzesiek, S., Vuister, G. W., Zhu, G., Pfeifer, J., and Bax, A. (1995) Nmrpipe: A Multidimensional Spectral Processing System Based on Unix Pipes. *J. Biomol. NMR 6*, 277–293.
49. Kneller, D. G., and Kuntz, I. D. (1993) Ucsf Sparky: An Nmr Display, Annotation and Assignment Tool. *J. Cell. Biochem.* 254–254.
50. Schleucher, J., Schwendinger, M., Sattler, M., Schmidt, P., Schedletzky, O., Glaser, S. J., Sorensen, O. W., and Griesinger, C. (1994) A General Enhancement Scheme in Heteronuclear Multidimensional NMR Employing Pulsed-Field Gradients. *J. Biomol. NMR 4*, 301–306.
51. Yamazaki, T., Muhandiram, R., and Kay, L. E. (1994) NMR Experiments for the Measurement of Carbon Relaxation Properties in Highly Enriched, Uniformly C-13,N-15-Labeled Proteins: Application to C-13(Alpha) Carbons. *J. Am. Chem. Soc. 116*, 8266–8278.
52. Korzhnev, D. M., Skrynnikov, N. R., Millet, O., Torchia, D. A., and Kay, L. E. (2002) An NMR experiment for the accurate measurement of heteronuclear spin-lock relaxation rates. *J. Am. Chem. Soc. 124*, 10743–10753.
53. Korzhnev, D. M., Billeter, M., Arseniev, A. S., and Orekhov, V. Y. (2001) NMR studies of Brownian tumbling and internal motions in proteins. *Prog. Nucl. Magn. Reson. Spectrosc. 38*, 197–266.
54. Hansen, A. L., and Al-Hashimi, H. M. (2007) Dynamics of large elongated RNA by NMR carbon relaxation. *J. Am. Chem. Soc. 129*, 16072–16082.
55. Loria, J. P., Rance, M., and Palmer, A. G. (1999) A relaxation-compensated Carr-Purcell-Meiboom-Gill sequence for characterizing chemical exchange by NMR spectroscopy. *J. Am. Chem. Soc. 121*, 2331–2332.
56. Mulder, F. A., Mittermaier, A., Hon, B., Dahlquist, F. W., and Kay, L. E. (2001) Studying excited states of proteins by NMR spectroscopy. *Nat. Struct. Biol. 8*, 932–935.
57. Wu, B., Petersen, M., Girard, F., Tessari, M., and Wijmenga, S. S. (2006) Prediction of molecular alignment of nucleic acids in aligned media. *J. Biomol. NMR 35*, 103–115.
58. Lu, X. J., and Olson, W. K. (2003) 3DNA: A software package for the analysis, rebuilding and visualization of three-dimensional nucleic acid structures. *Nucleic Acids Res. 31*, 5108–5121.
59. Stueber, D., and Grant, D. M. (2002) C-13 and N-15 chemical shift tensors in adenosine, guanosine dihydrate, 2′-deoxythymidine, and cytidine. *J. Am. Chem. Soc. 124*, 10539–10551.
60. de la Torre, J. G., Huertas, M. L., and Carrasco, B. (2000) HYDRONMR: Prediction of NMR relaxation of globular proteins from atomic-level structures and hydrodynamic calculations. *J. Magn. Reson. 147*, 138–146.
61. Mandel, A. M., Akke, M., and Palmer, A. G. (1995) Backbone Dynamics of *Escherichia coli* Ribonuclease Hi: Correlations with Structure and Function in an Active Enzyme. *J. Mol. Biol. 246*, 144–163.
62. Cromsigt, J. A. M. T. C., Hilbers, C. W., and Wijmenga, S. S. (2001) Prediction of proton chemical shifts in RNA: Their use in structure refinement and validation. *J. Biomol. NMR 21*, 11–29.
63. Nelissen, F. H. T., van Gammeren, A. J., Tessari, M., Girard, F. C., Heus, H. A., and Wijmenga, S. S. (2008) Multiple segmental and selective isotope labeling of large RNA for NMR structural studies. *Nucleic Acids Res. 36*, e89.
64. O'Neil-Cabello, E., Bryce, D. L., Nikonowicz, E. P., and Bax, A. (2004) Measurement of five dipolar couplings from a single 3D NMR multiplet applied to the study of RNA dynamics. *J. Am. Chem. Soc. 126*, 66–67.
65. Shajani, Z., and Varani, G. (2008) C-13 relaxation studies of the DNA target sequence for HhaI methyltransferase reveal unique motional properties. *Biochemistry 47*, 7617–7625.
66. Duchardt, E., Nilsson, L., and Schleucher, J. (2008) Cytosine ribose flexibility in DNA: A combined NMR C-13 spin relaxation and molecular dynamics simulation study. *Nucleic Acids Res. 36*, 4211–4219.